Analytical solution for two-phase flow in a wellbore using the drift-flux model

Lehua Pan[1*], Stephen W. Webb[2, 3], Curtis M. Oldenburg[1]

[1]Lawrence Berkeley National Laboratory

MS-9016, One Cyclotron Road, Berkeley, CA 94720, USA

[2]Sandia National Laboratories

New Mexico, PO Box 5800, Albuquerque, NM 87185

[3]currently at Canyon Ridge Consultants LLC

10 Canyon Ridge Dr., Sandia Park, NM 87047

- Corresponding author: LPAN@lbl.gov; Tel. 1-510-495-2360; Fax 1-510-486-5686

Abstract

This paper presents analytical solutions for steady-state, compressible two-phase flow through a wellbore under isothermal conditions using the drift flux conceptual model. Although only applicable to highly idealized systems, the analytical solutions are useful for verifying numerical simulation capabilities that can handle much more complicated systems, and can be used in their own right for gaining insight about two-phase flow processes in wells. The analytical solutions are obtained by solving the mixture momentum equation of steady-state, two-phase flow with an assumption that the two phases are immiscible. These analytical solutions describe the steady-state behavior of two-phase flow in the wellbore, including profiles of phase saturation, phase velocities, and pressure gradients, as affected by the total mass flow rate, phase mass fraction, and drift velocity (i.e., the slip between two phases). Close matching between the analytical solutions and numerical solutions for a hypothetical CO_2 leakage problem as well as to field data from a CO_2 production well indicates that the analytical solution is capable of capturing the major features of steady-state two-phase flow through an open wellbore, and that the related assumptions and simplifications are justified for many actual systems. In addition, we demonstrate the utility of the analytical solution to evaluate how the bottomhole pressure in a well in which CO_2 is leaking upward responds to the mass flow rate of CO_2-water mixture.

Keywords: Wellbore flow, analytical solution, two-phase flow, production from wells, geologic carbon sequestration, well leakage

1. Introduction

At its most basic level, management of subsurface resources involves a system comprising the wellbore and the target reservoir. As discrete pathways through geologic formations, boreholes and wells are critical to the success of many water, energy, and environmental management operations (e.g., geologic carbon sequestration, oil and gas production, compressed air energy storage, geothermal energy production, and subsurface remediation). Simulating two-phase flow in wellbores is an important, yet challenging, task required to answer critical questions on the design and performance of fluid production, injection, and transport systems. Because of the inherent difficulties in modeling two-phase flow with a two-fluid model (e.g., mathematical complications and uncertainties in specifying interfacial interaction terms between the two phases), the drift-flux model, which replaces the separated momentum equation for each phase by one momentum equation for the mixture as a whole complemented with the kinematic constitutive equations specifying the relative motion between phases, was proposed to significantly reduce these modeling difficulties ([1] Zuber and Findlay, 1965; [2] Nassos and Bankoff, 1967; [3] Ishii, 1977; [4] Wallis, 1969; [5] Hasan and Kabir, 1988; [6] Ansari et al., 1994; [7] Hibiki and Ishii, 2003; [8] Shi et al., 2005; [9] Ishii and Hibiki, 2006). However, even though the formulation of the drift-flux model is much simpler than the two-fluid model, the drift-flux equations are usually solved numerically mainly because of their nonlinear nature and complicated relationship between pressure and two-phase velocity fields. On the other hand, analytical solutions, if available, can be used to verify numerical modeling approaches and results. Wallis (1969) [4] presented a set of analytical solutions for steady-state homogeneous flow (i.e., no slip between the two phases). However, the slip between the two phases is the fundamental feature that makes two-phase flow different from single-phase flow, especially in terms of flow dynamics. Therefore, analytical solutions restricted to homogeneous flow

conditions provide limited insights into actual two-phase flow systems and have limited applications given the large number of two-phase flow situations such as those arising in wells involved with oil and gas, geothermal energy, and geologic carbon sequestration, among others.

In this work, we present an analytical procedure to solve the mixture momentum equation of steady-state, compressible, two-phase flow through a wellbore under isothermal conditions with certain simplifications. In addition, we demonstrate that the analytical solutions are useful for checking numerical model results for two-phase wellbore flow (through an open pipe) and for approximating some other practical wellbore processes such as gas leakage up wellbores.

2. The drift-flux model and the momentum equation for the mixture

In the following development, we assume the drift-flux model, which is limited to one-dimensional flow through an open pipe or annulus, is appropriate for describing steady-state two-phase flow and we develop an analytical solution to solving the drift-flux equations. Variables in the equations below pertaining to quantities normal to the flow direction should be considered as area-averaged or assumed to be constant over the cross-section except for those explicitly noted otherwise.

The drift-flux models were first developed by Zuber and Findlay (1965)[1] and Wallis (1969)[4] among others. Although various nomenclatures and forms of equations were used to describe the drift-flux model in the literature, the basic idea of the drift-flux models is to assume that the gas velocity, u_G, can be related to the volumetric flux of the mixture, j, and the drift velocity of gas, u_d, by the empirical constitutive relationship below:

$$u_G = C_0\, j + u_d \qquad (1)$$

where C_0 is the profile parameter to account for the effect of local gas saturation and velocity profiles over the pipe cross-section.

By definition, the volumetric flux j is the volumetrically weighted velocity

$$j = S_G u_G + (1 - S_G) u_L \qquad (2).$$

where S_G is the gas phase saturation. Therefore, the liquid velocity u_L can be determined as

$$u_L = \frac{1 - S_G C_0}{1 - S_G}\, j - \frac{S_G}{1 - S_G} u_d \qquad (3).$$

To simplify the problem, we assume that the profile effects over the cross-section are negligible ($C_0 = 1$) as is often the case for large-diameter pipe such as typical wellbores (Shi et al., 2005 [8]). Thus, the steady-state momentum equation of the mixture in a wellbore with uniform diameter can be written as follows (see Appendix A):

$$\frac{d}{dz}\left(\rho_m u_m^2 + \frac{S_G}{1 - S_G} \frac{\rho_G \rho_L}{\rho_m} u_d^2 \right) = -\frac{dP}{dz} - \frac{\Gamma f \rho_m |u_m| u_m}{2A} - \rho_m g \cos\theta \qquad (4)$$

Strictly speaking, two-phase flow occurs in different flow regimes resulting in different interfacial interactions. Shi et al. (2005) [8] proposed functional forms for the profile parameter and drift velocity that can be applied continuously for all flow regimes from bubble flow to annular film flow using a set of optimized parameters, obtained from an extensive set of large-scale pipe flow experiments performed by Oddie et al. (2003) [10] for one-, two-, and three-phase

flows at various inclinations. The following is a summary of the mathematical formulations related to the drift velocity proposed by Shi et al. (2005) [8] (simplified by $C_0 = 1$):

The drift velocity can be determined as a function of gas saturation, the characteristic velocity, u_c, the Kutateladze number, K_u (defined below), the density of gas phase, ρ_G, the density of liquid phase ρ_L, and the inclination adjustment, $m(\theta)$:

$$u_d = \frac{(1-S_G)u_c K(S_G, K_u) m(\theta)}{S_G\sqrt{\rho_G/\rho_L} + 1 - S_G} \qquad (5)$$

The "characteristic velocity," u_c , is a measure of the velocity of bubble rise in a liquid column, given by

$$u_c = \left[\frac{g\,\sigma_{GL}(\rho_L - \rho_G)}{\rho_L^2}\right]^{1/4} \qquad (6)$$

where σ_{GL} is the surface tension between gas and liquid phases and g is the acceleration of gravity.

K_u is the Kutateladze number, a function of Bond number, $N_B = d^2\left[\frac{g(\rho_L - \rho_G)}{\sigma_{GL}}\right]$, (Richter, 1981[11]):

$$K_u = \left[\frac{C_{ku}}{\sqrt{N_B}}\left(\sqrt{1 + \frac{N_B}{C_{ku}^2\, C_w}} - 1\right)\right]^{\frac{1}{2}} \qquad (7)$$

Where C_w is a wall friction factor, d is the wellbore diameter, and C_{ku} is a constant.

The function $K(S_G,K_u)$ in (5) is an interpolation function (from 1.53 to K_u) used to make a smooth transition of drift velocity between the bubble-rise stage and the film-flooding stage depending on gas saturation (Pan et al., 2009 [12]; Pan et al., 2011 [13]), which is similar to the interpolation proposed by Shi et al., (2005) except a nonlinear function is used to ensure that the first derivative is continue at the switch points.

Note that equation (5) described above cannot be applied to the mist flow regime, a special two phase flow pattern that often occurs at high velocity and high gas fraction, X. In the mist flow regime, the gas velocity is so high that the small amount of liquid (i.e., $X \approx 1$) cannot form a film but instead comprises tiny droplets that are uniformly distributed in the gas flow. As a result, the slip between the two phases in the mist flow regime diminishes. Cheng et al. (2008) [14] developed a flow pattern map for CO_2 that suggests that the mist flow regime occurs when mass velocity (i.e., the total mass flow rate per unit cross-sectional area, G, in this paper) reaches more than 300 kg/m^2/s at higher X. To account for this region, we suggest to add to equation (5) an adjustment function $f(G, X)$, a smooth function that quickly approaches zero as the state point in the G-X plane gets into the mist flow regime whereas it would equal one everywhere else (see Appendix B), and calculate the drift velocity as follows:

$$u_d = \frac{(1-S_G)\,u_c\,K(S_G,K_u)\,m(\theta)\,f(G,X)}{S_G\sqrt{\rho_G/\rho_L}+1-S_G} \tag{8}$$

Although the formulations for calculation of the drift velocity are quite complicated, the drift velocity is basically a function of S_g, ρ_g, and ρ_L for a given flow system (G and X).

3. Analytical solutions

At steady state, the total mass flow rate per unit cross-sectional area $G = \rho_m u_m$ is a constant and has units of flux, but for convenience we refer throughout to fluxes in the wellbore as flow rates. Therefore, the momentum Equation (4) can be rewritten as (assuming upward flow for simplicity):

$$\frac{d}{dz}\left(\frac{G^2}{\rho_m}+\frac{S_G}{1-S_G}\frac{\rho_G \rho_L}{\rho_m}u_d^2\right) = -\frac{dP}{dz} - \frac{\Gamma f G^2}{2A\rho_m} - \rho_m g\cos\theta \tag{9}$$

Further, because the solubility of each phase in the other phase is often very low in the systems we are considering, the mass fraction of the gas phase, *X*, is also independent of position and the densities only depend on pressures and temperature. Therefore, by definition, the gas saturation S_G (a volumetric fraction) and the mass fraction *X* can be related to the total mass flow rate as follows:

$$S_G = \frac{j_G}{j+u_d} = \frac{G X \big/ \rho_G}{G X \big/ \rho_G + G(1-X) \big/ \rho_L + u_d} = \frac{X}{X + a_1 \rho_G} \tag{10}$$

where $a_1 = \frac{1-X}{\rho_L} + \frac{u_d}{G}$. As a result, the mixture density ρ_m can be written as:

$$\rho_m = S_G \rho_G + (1-S_G)\rho_L = \frac{X\rho_G}{X + a_1\rho_G} + \frac{a_1 \rho_G \rho_L}{X + a_1 \rho_G} = \frac{\rho_G (X + a_1 \rho_L)}{X + a_1 \rho_G} \tag{11}$$

Or

$$\frac{1}{\rho_m} = \frac{a_1}{X + a_1 \rho_L} + \frac{X}{X + a_1 \rho_L} \cdot \frac{1}{\rho_G} \tag{12}$$

From (10), one can obtain the following useful relationship:

$$\frac{S_G}{1-S_G} = \frac{X}{a_1 \rho_G} \tag{13}$$

Because ρ_g, and ρ_L are functions of pressure and temperature here, combining Equations (8) and (10) together provides solution of S_G and u_d for a given pressure and temperature. Similarly, the mixture density, ρ_m, can be obtained using Equation (11). The derivative on the left-hand side of Equation (9), after inserting (13), can be expanded into two parts:

$$\frac{d}{dz}\left(\frac{h}{\rho_m}\right) = \frac{\partial}{\partial P}\left(\frac{h}{\rho_m}\right)\frac{dP}{dz} + \frac{\partial}{\partial T}\left(\frac{h}{\rho_m}\right)\frac{dT}{dz} \tag{14}$$

where $h = G^2 + \frac{m_G \rho_L}{a_1} u_d^2$. is a function of pressure and temperature, and T is temperature.

In a well with steady-state upward leakage, the temperature gradient tends to be small (a so-called enforced isothermal condition) because the energy carried by the fluid is often dominant over the heat exchange between the well and the surrounding formation except for a short period at early time. For a system with high heat capacity fluid (e.g., water), thermal gradients are also often negligible. However, if the dominant fluid is a gas or CO_2 the fluid temperature could decrease with decompression as it flows up the well. As a result, the temperature gradient, although still often much smaller than the ambient geothermal gradient, cannot be ignored. In this case, we can approximate the temperature profile along the flow path as piece-wise linear (i.e., $\frac{dT}{dz} = g_T$ is constant within each section) and the entire Equation (9) can be rewritten as:

$$\left(\frac{\partial}{\partial P}\left(\frac{h}{\rho_m}\right)+1\right)\frac{dP}{dz} = -\frac{\Gamma f G^2}{2A\rho_m} - \rho_m g \cos\theta - \frac{\partial}{\partial T}\left(\frac{h}{\rho_m}\right) g_T \tag{15}$$

By taking the T and g_t as parameters and integrating (15), we can obtain the following inverse of pressure distribution *z(P)*:

$$z(P) = z_0 - \int_{P_0}^{P} \frac{1 + \frac{\partial}{\partial P}\left(\frac{h}{\rho_m}\right)}{\frac{\Gamma f G^2}{2A\rho_m} + \rho_m g \cos\theta + \frac{\partial}{\partial T}\left(\frac{h}{\rho_m}\right) g_T} dP \qquad (16)$$

where P_0 is the pressure at the reference location z_0.

Although a closed-form function could not be obtained except for some special cases, the integration of (16) can be calculated using simple numerical integration because the integrand is a smooth function of P. The same solution methods could be used for the case of (mean) downward flow with a negative sign of the friction term because the directions of the friction force and the gravity force are opposite.

Note that analytical solutions to the momentum equations of the commonly used simpler models such as constant slip, no slip (i.e., homogeneous flow), or even single phase flow, are all special cases of (16).

Finally, a general procedure to obtain the analytical solutions can be summarized as follows:

Step 1: for a series of P (starting from P_0), calculate the corresponding $\rho_G(P,T)$ and $\rho_L(P,T)$, e.g., from equations of state or look-up tables.

Step 2: Solve S_G and u_d from Equations (8) and (10) for given ρ_G and ρ_L;

Step 3: Calculate ρ_m, $h(P)$, and the integrand of (16) at each P;

Step 4: calculate z(P) by integration of (16);

Step 5: Calculate u_m ($= G/\rho_m$) and other variables (e.g., components of pressure loss) at each point.

4. Results and discussions

4.1 Verification against numerical wellbore models

To verify the analytical solution developed above, we first compare the analytical solution to the results of a numerical wellbore flow simulator T2Well (Pan et al., 2009[12]; Pan et al., 2010[13]) which extends TOUGH2 (Pruess et al., 1999[15]) to handle wellbore flow. We consider an idealized problem of steady-state, isothermal, two-phase (air and water) flow through a vertical wellbore of 1000 m length. The details of the problem are described below (Table 1):

Table 1 Parameters of the two-phase wellbore flow problem

Parameter	Value for analytical solution	Value for numerical solution
Length	1000 m (vertical)	1000 m (vertical)
Diameter	0.1 m (circular)	0.1 m (circular)
Total (upward) mass flow rate	50 kg/m^2/s (gas + liquid)	air: 0.19625 kg/s; water: 0.19625 kg/s (Each = 25 kg/m^2/s with a cross sectional area of 7.85 $\times 10^{-3}$ m^2)
Gas mass fraction	0.5 ($=\frac{S_G \rho_G u_G}{G}$)	
Temperature	20 ℃ (isothermal)	20 ℃ (isothermal)
Wellhead Pressure	10^5 Pa	10^5 Pa

Wall roughness	2.4×10^{-5} m	2.4×10^{-5} m

The T2Well/EOS3 problem is run as a transient problem with adaptive time steps. The ending simulation time is 7.85×10^{8} seconds (4100 steps), at which the average time-derivative of momentum is about -2.2×10^{-17} (Pa/m) indicating an effective steady state was reached.

In the analytical solution, the gas and liquid phases are pure air and water, respectively, with the assumption that there is no mixing between the phases, i.e., the phases are immiscible, an assumption reasonably well-approximated by phases such as water and air, or brine and CO_2, and somewhat less so by oil and natural gas. The phase densities were calculated using the same methods as used in the full TOUGH2/EOS3 numerical solution for pure water and air. However, in the numerical solution, the gas and liquid phases consist of mixtures of water and air components as controlled by a local solubility model.

As shown in Figure 1, the agreement is very good between the numerical solution and the analytical solution. The almost perfect match (the coefficient of determination, $R^2 > 0.998$) between analytical solutions and the numerical solutions implies that the effects on the two-phase flow of the mixing modeled in TOUGH2 of the components in the phases are negligible, at least in this high gas-saturation system. Furthermore, the assumption of isothermal conditions in the analytical solution is justified because the upward-flowing well will quickly establish a nearly steady-state temperature profile with negligible gradient.

In this system, although the mass fraction is constant ($X = 0.5$) throughout the wellbore, the gas saturation decreases with depth due to pressure increase even though the gas saturation is high (> 0.82) because of the low density of air over the given pressure range (Figure 1). Meanwhile, the drift velocity (of the gas phase relative to the mean volumetric velocity) increases

with depth from about 0.2 m/s to 0.6 m/s. However, the gas phase velocity decreases with depth by about five times over 1000 meters (Figure 1).

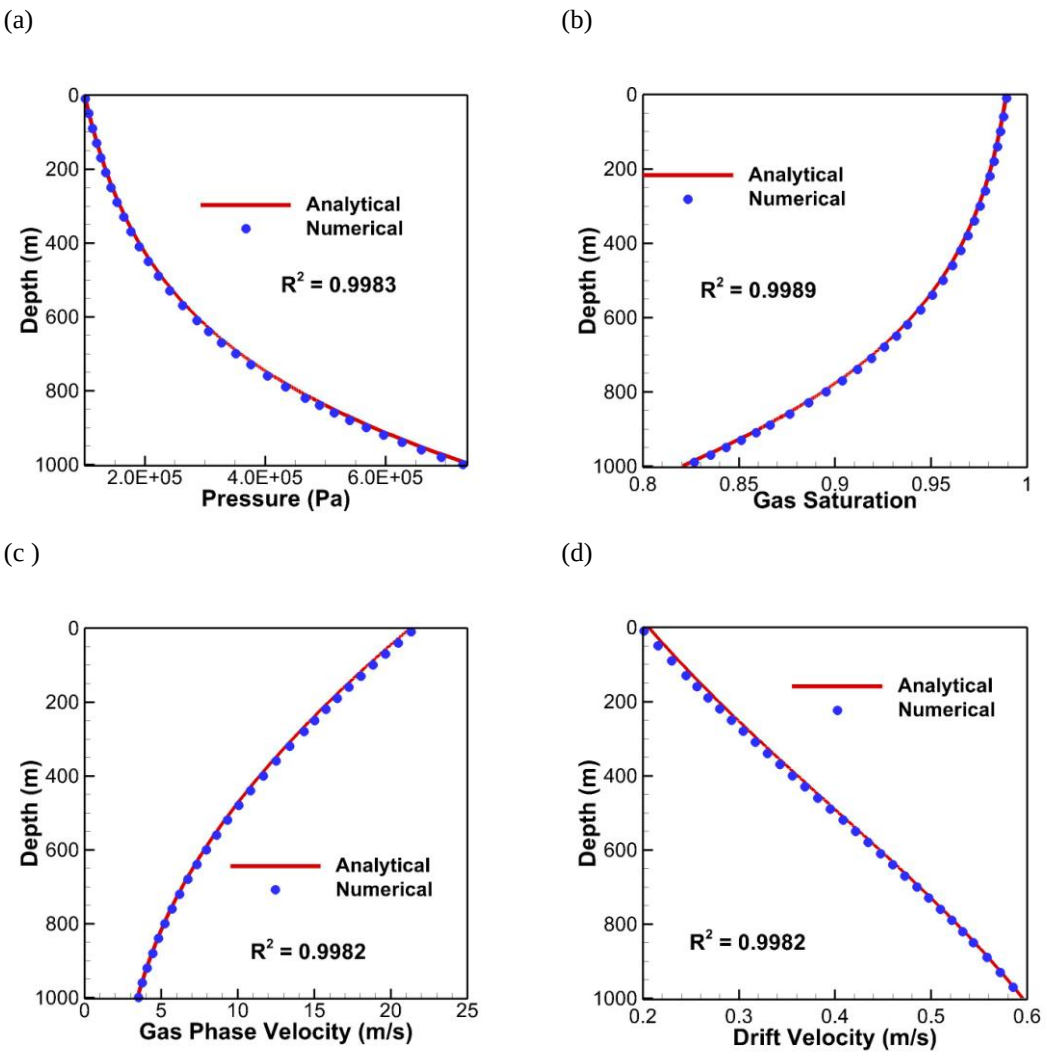

Figure 1. Depth profiles of pressure, gas saturation, gas-phase velocity, and drift velocity under steady-state, isothermal, two-phase (air/water) flow conditions in a vertical wellbore showing excellent agreement between analytical and numerical results. R^2 is the coefficient of determination.

4.2 Evaluating the effects of the drift velocity on flow in the wellbore

The analytical solution developed here can be used to gain significant insight into the effects of various assumptions about drift velocity and gas saturation. Figure 2 shows the analytical solutions of the same problem described in Section 4.1 but with different assumption for the drift velocity. The base case is the analytical solution where the drift velocity is calculated using Equation (8). The drift velocity of the base case increases almost linearly with depth from about 0.2 m/s to 0.6 m/s. If one assumes a constant drift velocity equal to the average value (= 0.4 m/s), the bottomhole pressure is very close to the base case although the pressure match in the middle regions of the well is slightly off. This holds true for the gas phase velocity also. However, in term of gas saturation, the difference is at the two ends of the borehole (wellhead or bottomhole). In general, the higher the drift velocity (u_d) is, the lower the gas phase velocity (u_G) and gas saturation (S_G) are. It is easy to understand the relationship between the drift velocity and the gas saturation because Equation (9) implies that the gas saturation is inversely proportional to the drift velocity at a given pressure. However, it is not that straightforward to understand why the gas-phase velocity would decrease as the drift velocity increases because the former is suppose to be linearly and positively proportional to the latter at given volumetric flux as shown in Equation (1). The key to understand the phenomena is that the volumetric flux is not the same if the drift velocity is different here. Let us rewrite Equation (1) as following by expressing the volumetric flux in terms of mass fraction (X), total mass flux (G) and densities of each phase:

$$u_G = j + u_d = \frac{XG}{\rho_G} + \frac{(1-X)G}{\rho_L} + u_d \tag{17}$$

While the gas-phase velocity is linearly proportional to the drift velocity, it is inversely related to the densities (mainly gas density) which will greatly decrease as pressure increases. As a result, the increase in the gas-phase velocity due to the increase of the drift velocity is

overwhelmingly wiped out by the decrease in the gas-phase velocity caused by the increase of pressure (in turn the densities of fluids) at the same depth. This also explains why assuming the average value of the drift velocity would have a similar effect on the patterns (i.e., results matching at the two ends) of the pressure profile and the gas-phase velocity profile as compared to the base case.

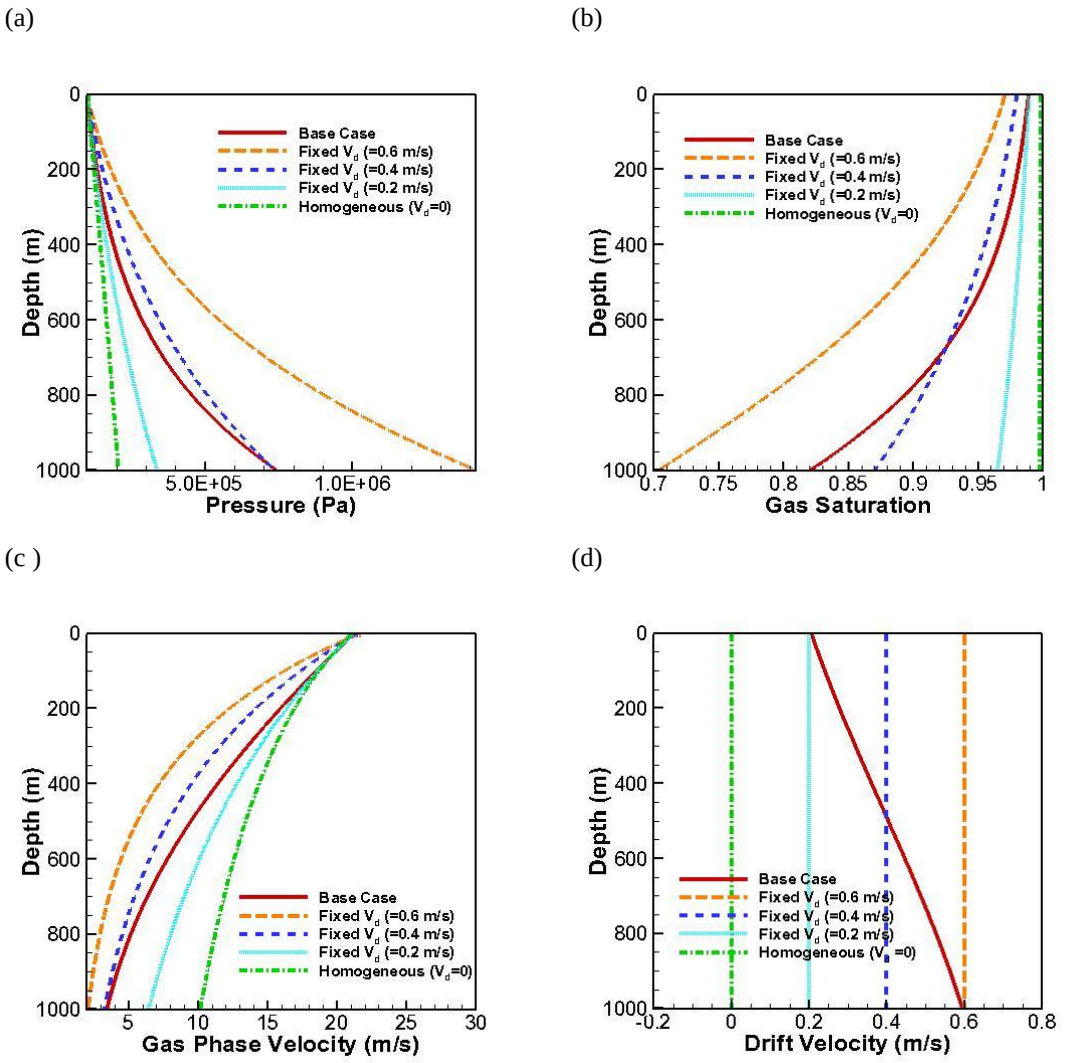

Figure 2. Effects of the drift velocity on the distribution of pressure, gas saturation, and gas-phase velocity. The base case is the same analytical solution as shown on Figure 1 where the drift velocity is calculated using Equation (5). The others assume that the drift velocity is constant over all depths.

In addition, higher drift velocity causes higher bottomhole pressure for a fixed wellhead pressure (Figure 2a). In other words, a larger pressure gradient is needed to maintain the same mass flow rate if the drift velocity is higher (Figure 3). Therefore, drift velocity (or slip) is a very important factor in simulating two phase flow problems and any simplification (e.g., assuming homogeneous flow or constant drift velocity) should be carefully evaluated because it may lead to a significant mis-estimation of total mass flow for a given pressure gradient.

Furthermore, as shown on Figure 3a, the total pressure gradient increases with depth except for the case of homogeneous flow and such increase is mainly caused by the hydrostatic pressure gradient (Figure 3b). Again, the drift velocity is positively related to the magnitude of such increase. Interestingly, the total pressure gradient in the homogeneous flow case decreases with increasing depth (Figure 3a). This is caused by the same trends in pressure gradients due to both friction loss to the wall and to acceleration (Figure 3c and 3d) while the hydrostatic pressure gradient is constant (Figure 3b) in the homogeneous case. For all other cases with non-zero drift velocity, the increase of hydrostatic pressure gradient with depth is a dominant factor over the others (comparing the values in Figure 3a and 3b), resulting in increase of total pressure gradient with depth. Note that the pressure gradient used to overcome the friction losses to the wall in the homogeneous flow case is much larger than those in the cases with non-zero drift velocity. This is because the no-slip condition between the two phases causes higher liquid-phase velocity, and in turn higher mixture velocity, for the same total mass flow rate in the homogeneous flow case (Figure 4).

(a)

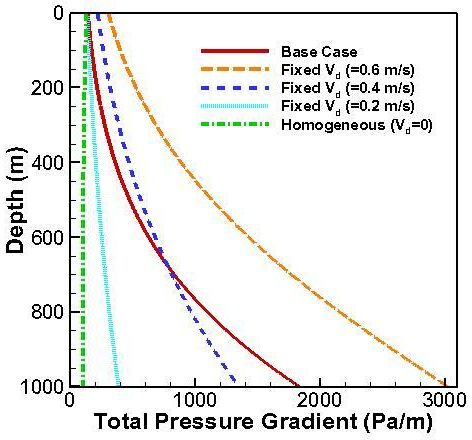

(b)

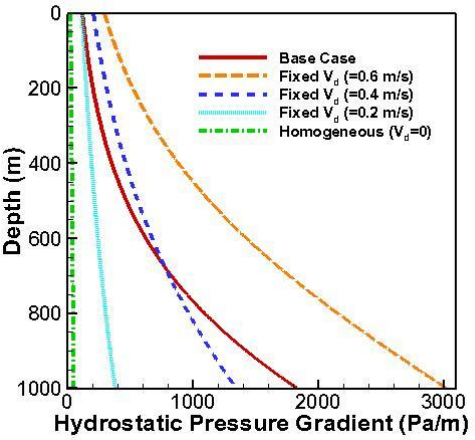

(c)

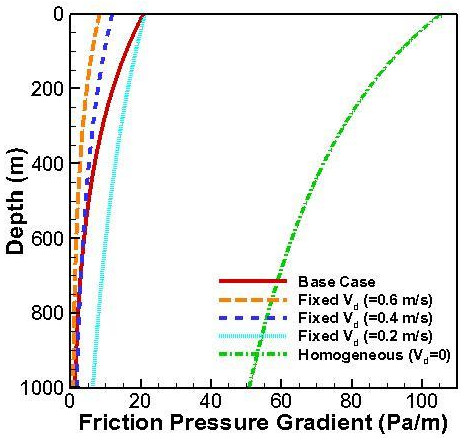

(d)

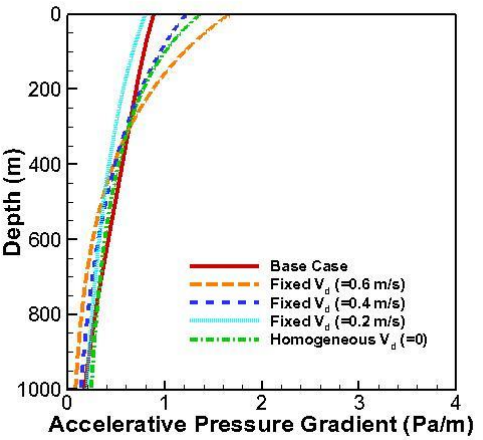

Figure 3. Effects of the drift velocity on the pressure gradients in a steady-state flow wellbore. The base case indicates the analytical solutions where the drift velocity is calculated using Equation (5).

(a) (b)

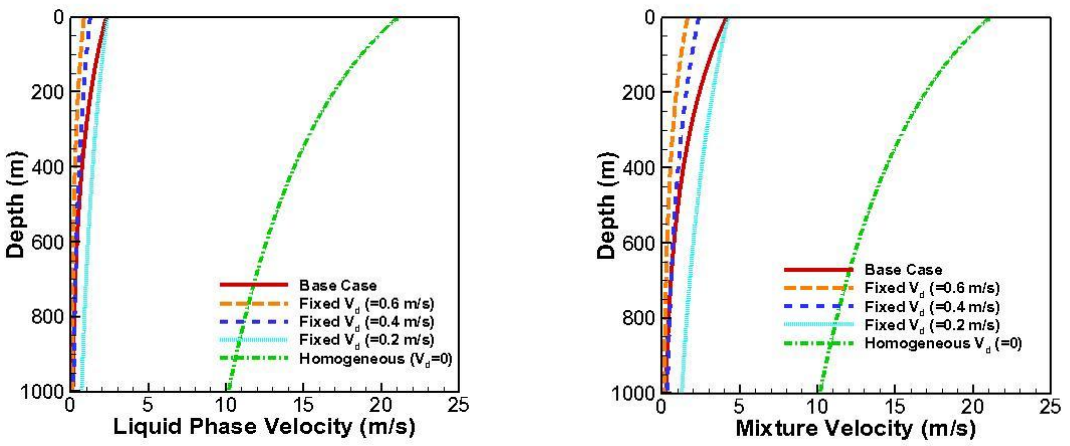

Figure 4 Effects of the drift velocity on the liquid velocity and the mixture velocity in a steady-state flow wellbore at the given total mass flow rate.

4.3 Validation with field CO_2 production test data

To demonstrate how well the analytical solution developed above could be used to describe wellbore flow in an actual well, in particular a well with vulnerable to potential CO_2 leakage, we compared our analytical solution to the field data of Cronshaw and Bolling (1982)[16]. Flow in the wellbore was believed to reach steady-state after half a day during a field production test (Cronshaw and Bolling, 1982) [16], and the pressure and temperature data were measured at that time. Totally four flow rates were used in the test. The well dimensions and other parameters are summarized in Table 2 (converted into SI units).

Table 2 Well dimensions and other parameters of the CO_2 production test problem.

Parameter	**Value**	**Note**
Length	914.4 m	Measured Depth
Diameter	0.088 m	Circular (tubing)

Incline angle	26.5 ^{o}		
Total (upward) mass flow rate	R1	408.95	Gas + Liquid Units: kg/m^2/s Corresponding to 2.5, 7.4, 11.2, and 13.7 kg/s per well, respectively
	R2	1210.03	
	R3	1827.46	
	R4	2230.20	
Gas mass fraction	0.97		Gas mass fraction is defined as equal to $\frac{S_G \rho_G u_G}{G}$
Temperature	From 15.5 to 43.0 ℃		Measured (8 points) temperature profile along the well for each flow rate
Bottom hole Pressure	R1	8.956	Unit: MPa
	R2	8.841	
	R3	8.709	
	R4	8.586	

The results of comparison of our analytical solution against measured field data for this problem are shown in Figure 5. The close match (the coefficient of determination is above 0.98 for all cases) between the analytical solutions and the measured data for varied flow rates indicates that the analytical solution, although strictly applicable only for an idealized system with many simplifications, can capture the major features of this complex CO_2-water upward flow system with an inclined wellbore, even though the system passes near the critical point of CO_2 during upward flow As the flow rate increases, the wellhead pressure decreases and the pressure gradient increases at every depth. Such a trend is mainly caused by the higher friction loss due to higher fluid velocity and compensated by the decreased hydrostatic loss due to lighter fluid mixture at lower pressure (Figure 6). As shown in Figure 6, the analytical solutions indicate that the friction and acceleration pressure gradient varies from very small values for lower flow

rate to a high values that are comparable to the hydrostatic pressure gradient for higher flow rate, although overall the hydrostatic pressure loss is still a major contribution. In this CO_2 dominant (97%) system, the temperature decreases as pressure decreases. This effect keeps the system close to the liquid-gas phase boundary when it becomes sub-critical. In terms of pressure loss, a lower temperature contributes to a higher density of CO_2 and in turn a higher hydrostatic pressure loss. However, the strong dependence of CO_2 density on pressure is still dominant so that the overall hydrostatic pressure gradient under higher flow rate is still smaller than that under lower flow rate (Figure6).

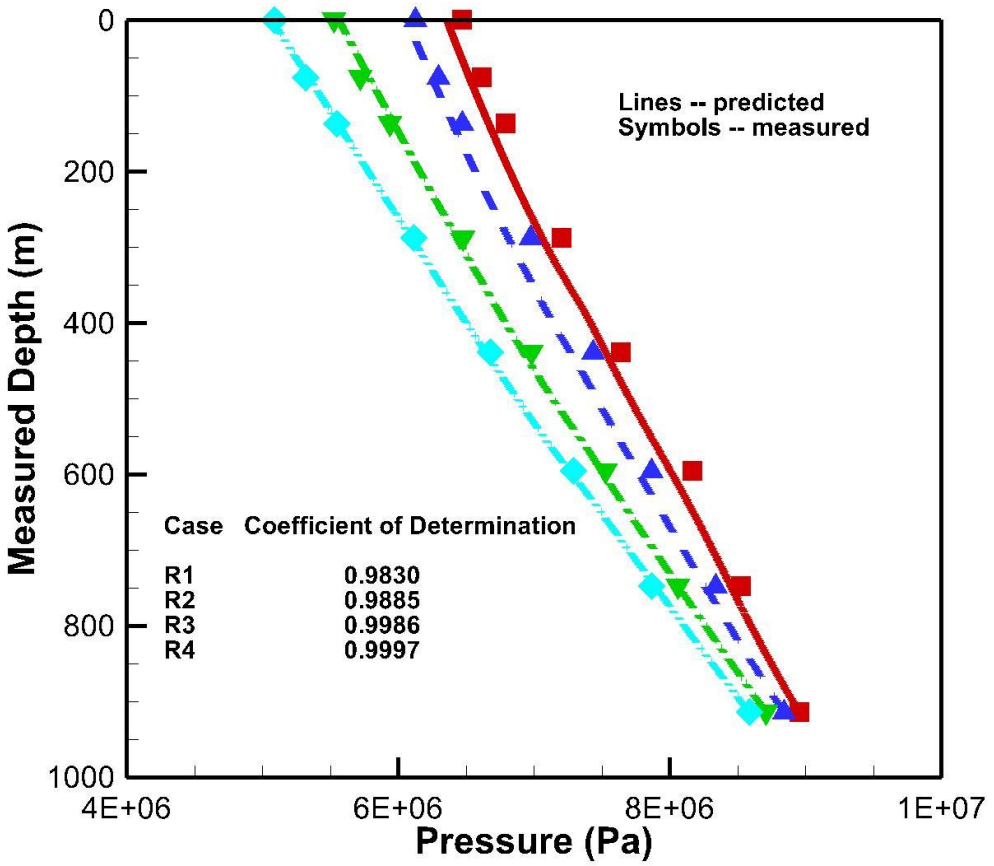

Figure 5 Results of analytical solution and measured pressures in a CO_2 production well under different flow rates (see Table 2). Lines are analytical solutions whereas the symbols are the measured data (red – R1; blue – R2; green – R3; and cyan – R4).

(a) (b)

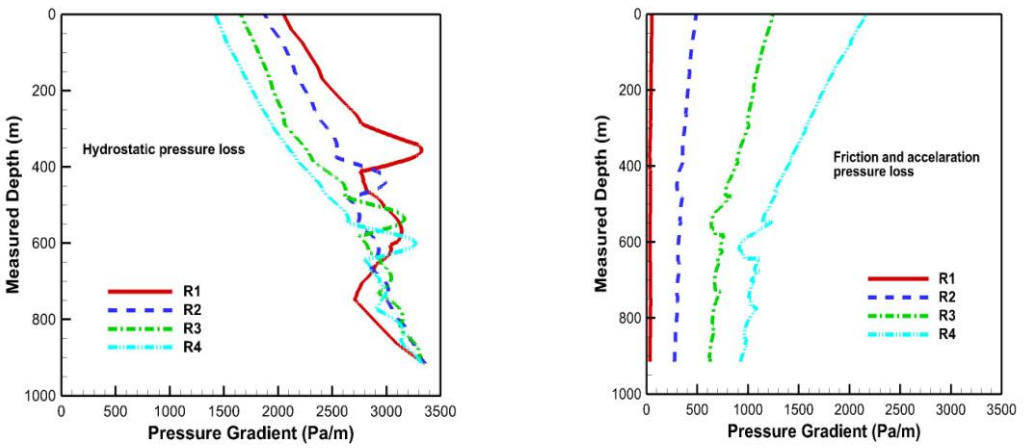

Figure 6. Analytical solutions of pressure gradients under various flow rates. a) hydrostatic; b) friction+acceleration. R1—2.5 kg/s; R2 – 7.4 kg/s; R3 – 11.2 kg/s; and R4 – 13.7 kg/s per well (diameter=0.088m).

4.4 Estimating the down hole pressure from two-phase leakage flow rate at the surface

In this example, we hypothesize a scenario in which CO_2 and water are leaking from a well and we show that the analytical solution can be used to estimate the down-hole (bottomhole) pressure from the measured steady-state leakage rates of CO_2 and water at the surface. The

relevance of this problem stems from the ongoing development and testing of the technology of geologic carbon sequestration, wherein CO_2 from large industrial and power-plant emission sources will be captured and injected deep underground to reduce CO_2 emissions to the atmosphere (e.g., IPCC, 2005 [17]). Despite the great depth, there is a chance that CO_2 could leak up wells that penetrate the storage region (e.g., Gasda et al., 2004 [18]; Pan et al., 2009 [12]). The specifications of the two-phase CO_2 leakage test problem are described in Table 3, and results are shown in Figure 7. Densities of pure CO_2 (including supercritical CO_2) and aqueous phases as a function of pressure and temperature used in the analytical solution were calculated using the same methods as in TOUGH2/ECO2N (Pruess and Spycher, 2007 [19]).

Table 3 Two-phase leakage problem (CO_2 and water).

Parameter	Value	Note
Length	1000 m	Vertical wellbore
Diameter	0.1 m	Circular
Gas flow rate	0.25-75 ($kg/m^2/s$)	2500 pairs of gas flow rate and liquid flow rate
Liquid flow rate	0 - 2500 ($kg/m^2/s$)	
Temperature	40 ℃	Isothermal
Wellhead Pressure	0.1 MPa	

As shown in Figure 7, the bottomhole pressure is very sensitive to the gas flow rate whereas it is sensitive to the liquid flow rate only when the gas flow is in the high range. The bottomhole pressure decreases as the gas flow rate increases. This is because with higher gas-flow rate, the gas saturation is higher and thus the mixture density is lower, resulting in less hydrostatic pressure at the bottom. As discussed in Section 4.2 (Figure 3), in such a vertical steady-state two-phase flow system, the hydrostatic pressure drop is often the dominant component of the overall pressure gradient, provided that the liquid phase has much higher density than the gas phase. However, this is not to say that a lower pressure plume would have a higher gas leakage rate through an open wellbore. Instead, the result only shows that a lower pressure gradient (thus a lower down-hole pressure because of the fixed wellhead pressure) is capable of sustaining a higher gas flow rate in the two-phase flowing well. Therefore, a higher pressure plume could drive more fluid into the well for a given bottomhole pressure, resulting in higher total flow rates of leakage. Here, one of the critical factors is the mass fraction of CO_2 in the plume, which greatly affects the steady-state ratio of gas to liquid phase flow rates. Similar to gas lifting, more gas could result in not only more gas flow but also more liquid flow. If the wellhead is at atmospheric pressure and the reservoir pressures is constant in the range of Figure 7, the contour lines of Figure 7 provide gas leakage rate as a function of liquid leakage rate, and vice versa.

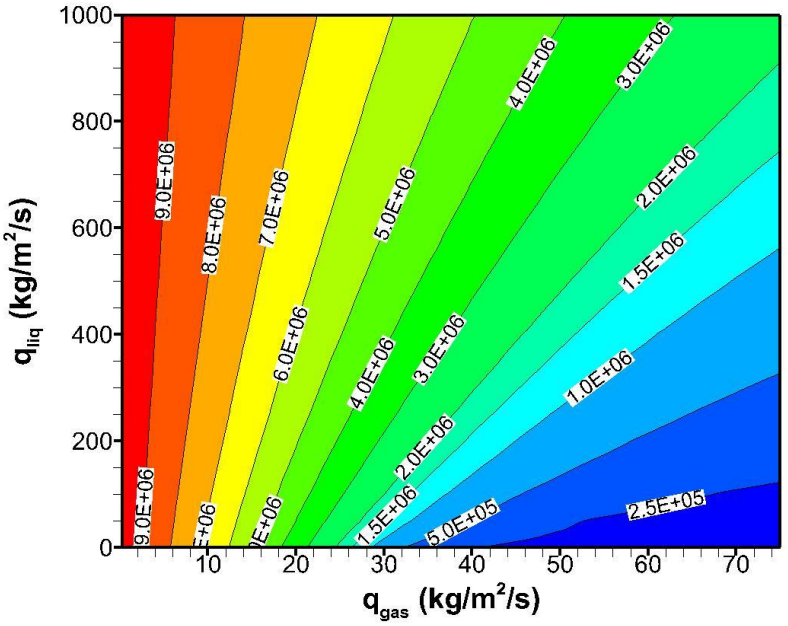

Figure 7 Contours of bottomhole pressure (Pa) as a function of the mass flow rates of gas and liquid for a well leaking a two-phase mixture of CO_2 and water.

5. Concluding remarks

This paper shows that with assumptions of negligible mixing between two phases and under isothermal conditions, it is possible to obtain analytical solutions for steady-state two phase flow through a wellbore using the drift-flux model. The resulting analytical solutions are more broadly applicable than prior solutions that assumed homogeneous flow (no slip between the two phases). As demonstrated in this work, these analytical solutions are useful for verifying numerical models

of two-phase flow in wellbores that can simulate a wide variety of flow processes including non-isothermal flows with multiple feed zones, condensation, boiling, and other fluid behaviors not amenable to analytical solutions. Although the new solutions also have some limiting assumptions, they can also be used to obtain insight into some fundamental two-phase flow processes in wellbores.

Appendix A: Derivation of momentum equation

All variables in the development below should be considered as area-averaged or assumed to be constant over the cross-section of a wellbore except for those explicitly noted otherwise.

The combined-phase momentum equation for wellbore (or duct) flow when the axial stress terms are assumed negligible can be written as (Brennen, 2005 [20]):

$$\frac{\partial}{\partial t}\left(\sum_{\beta}\rho_{\beta}\,S_{\beta}\,u_{\beta}\right)+\frac{1}{A}\frac{\partial}{\partial z}\left(A\sum_{\beta}\rho_{\beta}\,S_{\beta}\,u_{\beta}^{2}\right)=-\frac{\partial P}{\partial z}-\frac{\Gamma\,\tau_{w}}{A}-\rho_{m}\,g\cos\theta \qquad \text{(A1)}$$

where ρ is density, S is saturation, u is velocity, P is the pressure, A is cross sectional area of the wellbore, Γ, is the perimeter of the cross-section, τ_w is the wall shear stress, and θ is the local angle between wellbore section, and the vertical direction. Subscript β indicates phase and m indicates the mixture whereas t is time and z is spatial coordinate along the wellbore. Note that to be consistent with the drift-flux model, the area-averaged variable, P, is defined as the pressure of the mixture regardless if it is dispersed or film two phase flow because the uniform drift-flux model proposed by Shi et al. (2005) [8] is applied to all flow regimes with the same set of the optimized parameters obtained from fitting to experimental data.

The wall shear stress is the friction force between the fluids and the wellbore wall. This term depends on properties and velocities of both the gas and the liquid phases as well as their fractions of the contact area with the wall. Rigorously determining this term would involve figuring out the detailed two-phase flow structure near the wall, a difficult task that is intended to

be avoided by using the drift-flux model. We assume that the stress is proportional to the square of the mixture velocity:

$$\tau_w = \frac{1}{2} f \rho_m |u_m| u_m \qquad \text{(A2)}$$

where the Fanning friction coefficient (*f*) is a function of the Reynolds number (*Re*) (Brill and Mukherjee, 1999 [21], rewritten as Fanning friction coefficient):

$$f = \frac{16}{\mathrm{Re}} \qquad \text{for Re < 2400,}$$

$$\text{and } \frac{1}{\sqrt{f}} = -4\log\left[\frac{2\varepsilon/d}{3.7} - \frac{5.02}{\mathrm{Re}}\log\left(\frac{2\varepsilon/d}{3.7} + \frac{13}{\mathrm{Re}}\right)\right] \text{ for Re > 2400} \qquad \text{(A3)}$$

where ε is the roughness of the wellbore and the Reynolds number is defined as $\mathrm{Re} = \rho_m u_m d / \mu_m$ where μ_m is the mixture viscosity and *d* is the wellbore diameter.

Before deriving the momentum conservation equation for the mixture, let us define the mixture density, ρ_m, and the mixture velocity (velocity of mass centre), u_m, as follows:

$$\rho_m = S_G \rho_G + (1 - S_G)\rho_L \qquad \text{(A4)}$$

$$u_m = \frac{S_G \rho_G u_G + (1 - S_G)\rho_L u_L}{\rho_m} \qquad \text{(A5)}$$

By inserting (1) and (3) into (A5), we can solve *j* as a function of u_m and u_d:

$$j = \frac{\rho_m}{\rho_m^*} u_m + \frac{S_G(\rho_L - \rho_G)}{\rho_m^*} u_d \qquad \text{(A6)}$$

Where $\rho_m^* = S_G C_0 \rho_G + (1 - S_G C_0)\rho_L$ is the profile-adjusted average density and will reduce to the mixture density if $C_0 = 1$. Note that the mixture velocity and the volumetric flux of

the mixture would be equal only if there is no slip between two phases (i.e., C_0 =1.0 and u_d = 0.0 or homogeneous flow).

Similarly, the gas velocity and the liquid velocity can also be expressed in terms of u_m and u_d as follows:

$$u_G = C_0 \frac{\rho_m}{\rho_m^*} u_m + \frac{\rho_L}{\rho_m^*} u_d$$
$$u_L = \frac{(1-S_G C_0)\rho_m}{(1-S_G)\rho_m^*} u_m - \frac{S_G \rho_G}{(1-S_G)\rho_m^*} u_d \qquad \text{(A7)}$$

By inserting the stress term (A2) and the phase velocities (A7) into (A1), we can obtain the momentum equation in terms of the mixture velocity u_m and the drift velocity u_d:

$$\frac{\partial}{\partial t}(\rho_m u_m) + \frac{1}{A}\frac{\partial}{\partial z}\left[A(\rho_m u_m^2 + \gamma)\right] = -\frac{\partial P}{\partial z} - \frac{\Gamma f \rho_m |u_m| u_m}{2A} - \rho_m g \cos\theta \quad \text{(A8)}$$

where the term $\gamma = \frac{S_G}{1-S_G}\frac{\rho_G \rho_L \rho_m}{\rho_m^{*2}}\left[(C_0 - 1)u_m + u_d\right]^2$ is caused by slip between two phases.

While other terms in (A8) are straightforward, the second term on the left is obtained as below:

$$\sum_{\beta}\rho_{\beta}S_{\beta}u_{\beta}^{2}=S_{G}\rho_{G}u_{G}^{2}+(1-S_{G})\rho_{L}u_{L}^{2}$$

$$=S_{G}\rho_{G}\left[C_{0}\frac{\rho_{m}}{\rho_{m}^{*}}u_{m}+\frac{\rho_{L}}{\rho_{m}^{*}}u_{d}\right]^{2}+(1-S_{G})\rho_{L}\left[\frac{(1-S_{G}C_{0})\rho_{m}}{(1-S_{G})\rho_{m}^{*}}u_{m}-\frac{S_{G}\rho_{G}}{(1-S_{G})\rho_{m}^{*}}u_{d}\right]^{2}$$

$$=u_{m}^{2}\left(\frac{S_{G}\rho_{G}C_{0}^{2}\rho_{m}^{2}}{\rho_{m}^{*2}}+\frac{\rho_{L}\rho_{m}^{2}(1-S_{G}C_{0})^{2}}{(1-S_{G})\rho_{m}^{*2}}\right) \qquad \text{(A9)}$$

$$+2u_{m}u_{d}\left(\frac{S_{G}\rho_{G}\rho_{L}\rho_{m}C_{0}}{\rho_{m}^{*2}}-\frac{S_{G}\rho_{G}\rho_{L}\rho_{m}(1-S_{G}C_{0})}{(1-S_{G})\rho_{m}^{*2}}\right)$$

$$+u_{d}^{2}\left(\frac{S_{G}\rho_{G}\rho_{L}^{2}}{\rho_{m}^{*2}}+\frac{\rho_{L}S_{G}^{2}\rho_{G}^{2}}{(1-S_{G})\rho_{m}^{*2}}\right)$$

In (A9), the u_{m}^{2} term can be reorganized as follow:

$$\rho_{m}u_{m}^{2}-\rho_{m}u_{m}^{2}+u_{m}^{2}\left(\frac{S_{G}\rho_{G}C_{0}^{2}\rho_{m}^{2}}{\rho_{m}^{*2}}+\frac{\rho_{L}\rho_{m}^{2}(1-S_{G}C_{0})^{2}}{(1-S_{G})\rho_{m}^{*2}}\right)=$$

$$=\rho_{m}u_{m}^{2}+\frac{\rho_{m}u_{m}^{2}}{(1-S_{G})\rho_{m}^{*2}}\left[S_{G}\rho_{G}(1-S_{G})\rho_{m}C_{0}^{2}+\rho_{L}\rho_{m}(1-S_{G}C_{0})^{2}-(1-S_{G})\rho_{m}^{*2}\right] \qquad \text{(A10)}$$

By expanding ρ_{m}^{*} and recognizing the relationship (A4), the term in [.] of (A10) can be simplified as:

$$S_{G}\rho_{G}(1-S_{G})\rho_{m}C_{0}^{2}+\rho_{L}\rho_{m}(1-S_{G}C_{0})^{2}-(1-S_{G})\rho_{m}^{*2}=$$

$$=S_{G}\rho_{G}(1-S_{G})\rho_{m}C_{0}^{2}+\rho_{L}\rho_{m}(1-S_{G}C_{0})^{2}-(1-S_{G})\left[S_{G}^{2}\rho_{G}^{2}C_{0}^{2}+\rho_{L}^{2}(1-S_{G}C_{0})^{2}+2S_{G}\rho_{G}C_{0}\rho_{L}(1-S_{G}C_{0})\right]=$$

$$=(1-S_{G})S_{G}\rho_{G}C_{0}^{2}(\rho_{m}-S_{G}\rho_{G})+\rho_{L}(1-S_{G}C_{0})^{2}(\rho_{m}-(1-S_{G})\rho_{L})-2S_{G}\rho_{G}C_{0}(1-S_{G})\rho_{L}(1-S_{G}C_{0})=$$

$$=S_{G}\rho_{G}\rho_{L}\left[(1-S_{G})^{2}C_{0}^{2}+(1-S_{G}C_{0})^{2}-2C_{0}(1-S_{G})(1-S_{G}C_{0})\right]=$$

$$=S_{G}\rho_{G}\rho_{L}\left[(1-S_{G})C_{0}-(1-S_{G}C_{0})\right]^{2}=S_{G}\rho_{G}\rho_{L}(C_{0}-1)^{2}$$

(A11)

Similarly, the $2u_{m}u_{d}$ term in (A9) can be simplified as:

$$2u_m u_d\left(\frac{S_G\rho_G\rho_L\rho_m C_0}{\rho_m^{*2}}-\frac{S_G\rho_G\rho_L\rho_m(1-S_G C_0)}{(1-S_G)\rho_m^{*2}}\right)=$$
$$=\frac{2u_m u_d S_G\rho_G\rho_L\rho_m}{(1-S_G)\rho_m^{*2}}[(1-S_G)C_0-(1-S_G C_0)]=\frac{2u_m u_d S_G\rho_G\rho_L\rho_m}{(1-S_G)\rho_m^{*2}}(C_0-1) \quad \text{(A12)}$$

And the u_d^2 term can be simplified as:

$$u_d^2\left(\frac{S_G\rho_G\rho_L^2}{\rho_m^{*2}}+\frac{\rho_L S_G^2\rho_G^2}{(1-S_G)\rho_m^{*2}}\right)=\frac{S_G\rho_G\rho_L u_d^2}{(1-S_G)\rho_m^{*2}}[((1-S_G)\rho_L+S_G\rho_G)]=\frac{S_G\rho_G\rho_L\rho_m u_d^2}{(1-S_G)\rho_m^{*2}} \quad \text{(A13)}$$

Putting together (A10) through (A13) into (A9), we obtain:

$$\sum_\beta \rho_\beta S_\beta u_\beta^2=\rho_m u_m^2+\frac{S_G\rho_G\rho_L\rho_m}{(1-S_G)\rho_m^{*2}}\left[(C_0-1)^2u_m^2+2(C_0-1)u_m u_d+u_d^2\right]=$$
$$=\rho_m u_m^2+\frac{S_G\rho_G\rho_L\rho_m}{(1-S_G)\rho_m^{*2}}[(C_0-1)u_m+u_d]^2=\rho_m u_m^2+\gamma \quad \text{(A14)}$$

Note that eq. (A8) is equivalent to the mixture moment equation for the drift model proposed by Hibiki and Ishii (2003) when the axial stress terms are assumed negligible. When all phases travel at the same velocity (i.e., $C_0=1 \text{ and } u_d=0$), γ will become zero and Eq. (A8) will reduce to the same momentum equation as a single phase flow. When steady state is reached and C_0 = 1, the momentum equation (A8) for flow in a uniform wellbore will be reduced to an ordinary differential Equation (4).

Appendix B. Adjustment function *f(G, X)* used in Equation (8).

The function *f(G, X)* is a continuous weighting function defined on the flow pattern map (*G*-*X*) developed by Cheng et al. (2008, Figure 3) in which *G* is flux (kg m^{-2} s^{-1}) and

X is gas mass fraction It shall be zero in the mist flow region where the drift velocity become effectively zero and increases quickly to 1 as the system moves away from mist region where the Shi model of drift velocity (Eq. 5 in main text) is optimized.

We simplified the mist flow region boundary on the flow pattern map as a straight line which is defined by its two end coordinates (X_{m1}, G_{m1}), (X_{m2}, G_{m2}). A given flow system with a mass flow rate *G* and mass fraction of gas *X* plots as a point on the flow pattern map. Therefore, how far a flow system (G, X) is away from the mist flow region can be measured by the distance from the state point (G, X) to the mist region boundary, (X_{m1}, G_{m1})-(X_{m2}, G_{m2}). According to computational geometry, this distance, D_m (from a point to a straight line), can be calculated as:

$$D_m = \frac{\begin{vmatrix} X & \alpha G & 1 \\ X_{m1} & \alpha G_{m1} & 1 \\ X_{m2} & \alpha G_{m2} & 1 \end{vmatrix}}{\left[\left(X_{m2} - X_{m1} \right)^2 + \left(\alpha G_{m2} - \alpha G_{m1} \right)^2 \right]^{\frac{1}{2}}} \qquad \text{(B1)}$$

where α is the scaling factor for mass flow rate and $|\bullet|$ is the determinant of the matrix. The D_m will become a negative value when (G, X) is inside of the mist flow region and will increase as the point is ways from the mist flow region.

Finally, the adjustment function is defined as:

$$f(G, X) = \max\left[0.0, 1.0 - \min\left(1, \frac{G}{G_{m1}} \right) \exp\left(-\lambda D_m \left| D_m \right| \right) \right] \qquad \text{(B2)}$$

where λ is a fitting parameter controlling the steepness of the function and the term $\frac{G}{G_{m1}}$ accounts for the fact that the mist flow region only occurs in the high-velocity region (Cheng et al., 2008, Figure 3). The values of the parameters are shown in Table B1.

Table B1 parameters used for adjustment function

Parameter	Value
X_{m1}	1.0
X_{m2}	0.94
G_{m1}	300 kg/m^2/s
G_{m2}	700 kg/m^2/s
α	0.001 m^{2}s/kg
λ	199

Acknowledgments

This work was supported in part by the CO_2 Capture Project (CCP) of the Joint Industry Program (JIP), by the National Risk Assessment Partnership through the Assistant Secretary for Fossil Energy, Office of Sequestration, Hydrogen, and Clean Coal Fuels, National Energy Technology Laboratory (NETL), and by Lawrence Berkeley National Laboratory under Department of Energy Contract No. DE-AC02-05CH11231. We thank James E. Houseworth (LBNL) for comments on an earlier draft, and three anonymous reviewers who provided comments that helped us improve the paper.

References

[1] Zuber, N., and J.A. Findlay, 1965, Average volumetric concentration in two-phase flow systems, J. Heat Transfer ASME, 87(4), 453-468.

[2] Nassos, G.B. and S.G. Bankoff, 1967. Slip velocity ratios in air-water system under steady-state and transient conditions. Chem. Eng. Sci. 22:661.

[3] Ishii, M., 1977. One-dimensional drift-flux model and constitutive equations for relative motion between phases in various two-phase flow regimes. Argonne National Laboratory Report (October 1977) ANL-77-47.

[4] Wallis, G.B., 1969, One-dimensional Two-phase Flow, McGraw-Hill Book Company, New York.

[5] Hasan, A. R., and C. S. Kabir, 1992. Two-phase flow in vertical and inclined annuli. Int. J Multiphase flow 18(2):279-293.

[6] Ansari A.M., et al., 1994. A comprehensive mechanistic model for upward two-phase flow in wellbores. SPEPF (May 1994) 143; Trans. AIME, 297.

[7] Hibiki, T. and M. Ishii, 2003. One-dimensional drift-flux model and constitutive equations for relative motion between phases in various two-phase flow regimes. Int. J Multiphase flow 46:4935-4948.

[8] Shi, H., J.A. Holmes, L.J. Durlofsky, K. Aziz, L.R. Diaz, B. Alkaya, and G. Oddie, 2005, Drift-flux modeling of two-phase flow in wellbores, Soc. Pet. Eng. J., 24-33.

[9] Ishii, M., and T. Hibiki, 2006. Thermo-fluid Dynamics of Two-Phase Flow, Springer.

[10] Oddie, G., Shi, H., Durlofsky, L.J., Aziz, K., Pfeffer, B., Holmes, J.A., 2003. Experimental study of two and three phase flows in large diameter inclined pipes. Int. J Multiphase Flow 29:527–558.

[11] Richter, H.J., 1981, "Flooding in Tubes and Annuli", Int. J. Multiphase Flow, 7(6):647-658.

[12] Pan, L., C.M. Oldenburg, Y.-S. Wu, and K. Pruess, 2009. Wellbore flow model for carbon dioxide and brine, Energy Procedia, 1(1), 71-78, Proceedings of GHGT9, Nov. 16-20, 2008, Washington DC. LBNL-1416E.

[13] Pan, L., C.M. Oldenburg, and K. Pruess, 2010. T2Well/ECO2N Version 1.0: Multiphase and Non-Isothermal Model for Coupled Wellbore-Reservoir Flow of Carbon Dioxide and Water. LBNL-4291E.

[14] Cheng, L., G. Ribatski, J. M. Quiben, J. R. Thome, 2008. New prediction methods for CO2 evaporation inside tubes: Part I – A two-phase flow pattern map and a flow pattern based phenomenological model for two-phase flow frictional pressure drops. Int. J Heat and Mass Transfer 51: 111–124.

[15] Pruess, K., C.M. Oldenburg and G.J. Moridis, 1999. TOUGH2 User's Guide Version 2. E. O. Lawrence Berkeley National Laboratory Report *LBNL-43134*.

[16] Cronshaw, M. B., and J. D. Bolling, 1982. A numerical model of the non-isothermal flow of carbon dioxide in wellbores. In: SPE 10735, SPE California Regional Meeting, San Francisco, May 22-26.

[17] IPCC Special Report on Carbon Dioxide Capture and Storage, 2005. B. Metz, O. Davidson, H.C. de Coninck, M. Loos and L.A. Meyer, Editors,. Prepared by Working Group III of the Intergovernmental Panel on Climate Change, Cambridge University Press, Cambridge, UK.

[18] Gasda, SE, S Bachu and MA Celia, 2004. Spatial characterization of the location of potentially leaky wells penetrating a deep saline aquifer in a mature sedimentary basin, Environ. Geology, 46, 707-720.

[19] Pruess, K., and N. Spycher, ECO2N – A fluid property module for the TOUGH2 code for studies of CO_2 storage in saline formations, Energy Conversion and Management 48, 1761-1767, 2007.

[20] Brennen,, C. E. 2005. Fundamentals of multiphase flows. Cambridge University Press, pp 34-35.

[21] Brill and Mukherjee, 1999. Multiphase flow in wells, SPE Monograph Series, Vol. 17, Page 7, eq. 2.19.

.

Figure Captions

Figure 1. Depth profiles of pressure, gas saturation, gas-phase velocity, and drift velocity under steady-state, isothermal, two-phase (air/water) flow conditions in a vertical wellbore showing excellent agreement between analytical and numerical results.

Figure 2. Effects of the drift velocity on the distribution of pressure, gas saturation, and gas-phase velocity. The base case is the same analytical solution as shown on Figure 1 where the drift velocity is calculated using Equation (5). The others assume that the drift velocity is constant over all depths.

Figure 3. Effects of the drift velocity on the pressure gradients in a steady-state flow wellbore. The base case indicates the analytical solutions where the drift velocity is calculated using Equation (5).

Figure 4. Effects of the drift velocity on the liquid velocity and the mixture velocity in a steady-state flow wellbore at the given total mass flow rate.

Figure 5 Results of analytical solution and measured pressures in a CO_2 production well under different flow rates (see Table 2). Lines are analytical solutions whereas the symbols are the measured data (red – R1; blue – R2; green – R3; and cyan – R4).

Figure 6. Analytical solutions of pressure gradients under various flow rates. a) hydrostatic; b) friction+acceleration. R1—2.5 kg/s; R2 – 7.4 kg/s; R3 – 11.2 kg/s; and R4 – 13.7 kg/s per well (diameter=0.088m).

Figure 7. Contours of bottomhole pressure (Pa) as a function of the mass flow rates of gas and liquid for a well leaking a two-phase mixture of CO_2 and water.

Tables

Table 1 Parameters of the two-phase wellbore flow problem

Parameter	Value for analytical solution	Value for numerical solution
Length	1000 m (vertical)	1000 m (vertical)
Diameter	0.1 m (circular)	0.1 m (circular)
Total (upward) mass flow rate	50 $kg/m^2/s$ (gas + liquid)	air: 0.19625 kg/s; water: 0.19625 kg/s (Each = 25 $kg/m^2/s$ with a cross sectional area of 7.85×10^{-3} m^2)
Gas mass fraction	0.5 ($=\frac{S_G \rho_G u_G}{G}$)	
Temperature	20 ℃ (isothermal)	20 ℃ (isothermal)
Wellhead Pressure	10^5 Pa	10^5 Pa
Wall roughness	2.4×10^{-5} m	2.4×10^{-5} m

Table 2 Well dimensions and other parameters of the CO_2 production test problem.

Parameter	**Value**	**Note**
Length	914.4 m	Measured Depth
Diameter	0.088 m	Circular (tubing)

Incline angle	26.5 ^{o}		
Total (upward) mass flow rate	R1	408.95	Gas + Liquid Units: kg/m^2/s Corresponding to 2.5, 7.4, 11.2, and 13.7 kg/s per well, respectively
	R2	1210.03	
	R3	1827.46	
	R4	2230.20	
Gas mass fraction	0.97		Gas mass fraction is defined as equal to $\frac{S_G \rho_G u_G}{G}$
Temperature	From 15.5 to 43.0 ℃		Measured (8 points) temperature profile along the well for each flow rate
Bottom hole Pressure	R1	8.956	Unit: MPa
	R2	8.841	
	R3	8.709	
	R4	8.586	

Table 3 Two-phase leakage problem (CO_2 and water).

Parameter	Value	Note
Length	1000 m	Vertical wellbore
Diameter	0.1 m	Circular
Gas flow rate	0.25-75 (kg/m^2/s)	2500 pairs of gas flow rate and liquid flow rate
Liquid flow rate	0 - 2500 (kg/m^2/s)	
Temperature	40 ℃	Isothermal

Wellhead Pressure	0.1 MPa	